Investigation of fullerene cluster growth mechanisms by carbon atom addition using classical molecular dynamics

A. Allouch, J. Mougenot, A. Michau, S. Prasanna, Pascal Brault, F. Maurel, K. Hassouni

The Journal of Chemical Physics

RESEARCH ARTICLE | OCTOBER 20 2023

Investigation of fullerene cluster growth mechanisms by carbon atom addition using classical molecular dynamics

A. Allouch ; J. Mougenot ; A. Michau ; S. Prasanna ; P. Brault ; F. Maurel ; K. Hassouni

J. Chem. Phys. 159, 154303 (2023)
https://doi.org/10.1063/5.0166116

AIP Publishing

The Journal of Chemical Physics ARTICLE pubs.aip.org/aip/jcp

Investigation of fullerene cluster growth mechanisms by carbon atom addition using classical molecular dynamics

Cite as: J. Chem. Phys. 159, 154303 (2023); doi: 10.1063/5.0166116
Submitted: 3 July 2023 • Accepted: 28 September 2023 •
Published Online: 20 October 2023

A. Allouch,[1,a)] J. Mougenot,[1] A. Michau,[1] S. Prasanna,[1] P. Brault,[2] F. Maurel,[3] and K. Hassouni[1]

AFFILIATIONS

[1] Laboratoire des Sciences des Procédés et des Matériaux (LSPM), CNRS UPR 3407, Université Sorbonne Paris Nord, Villetaneuse, France
[2] Groupe de Recherches sur l'Energétique des Milieux Ionisés, CNRS UMR 7344, Université d'Orléans, Orléans, France
[3] Laboratoire Interfaces, Traitements, Organisation et Dynamique des Systèmes (ITODYS), UMR 7086, Université Paris Diderot, Paris, France

[a)] **Author to whom correspondence should be addressed:** amal.allouch@lspm.cnrs.fr

ABSTRACT

The mechanisms of carbon sticking reactions to C_{36} and $C–C_{80}$ fullerenes were investigated with molecular dynamics simulations (MD) using the Second-generation Reactive Empirical Bond Order (SREBO) and Adaptive Intermolecular Reactive Empirical Bond Order (AIREBO) potentials that were specifically optimized for carbon-carbon interactions. Results showed the existence of three possible sticking configurations where the projectile atom can stick either to one, two or three atoms of the target fullerene. They also showed that although the two potentials give similar magnitudes for the sticking cross-sections, they yield fairly different results as far as sticking mechanisms and configurations at thermal collision-energies, i.e., in the range 0.05–0.5 eV, are concerned. While AIREBO, that takes into account the long-range Lennard-Jones interaction, essentially results in a surface-sticking configuration with a single atom of the target fullerene, SREBO potential yields both surface- and two neighbors-sticking (2N-sticking) configurations. The fullerene structure is preserved in the last configuration while it can be recovered by a 2000 K annealing in the former configuration. Results obtained with SREBO eventually showed larger sticking probabilities for C_{36} as compared with C_{80}. In spite of this, the sticking cross-sections obtained for C_{80} are similar to or even larger than those obtained for C_{36} due to the larger size of C_{80} that compensates for its smaller sticking probabilities.

I. INTRODUCTION

The study of the properties of intermediate and large carbon clusters, C_n with $n > 32$, especially with even number of carbons, is of great interest due to the potential applications of these clusters in a variety of fields, such as nanotechnology and biomedicine (Bratovcic 2023, Paukov *et al.*, 2023; Perez-Mellor *et al.*, 2022; Rao *et al.*, 2021; Yang *et al.*, 2022). Carbon nanostructures are produced by gas phase nucleation which represents the fundamental principle underlying their synthesis process (Afanas'ev *et al.*, 2001; Alekseev *et al.*, 2001; Borand *et al.*, 2021; Farhat and Scott 2006). In particular, carbon clusters can be obtained at low temperature in non-equilibrium glow discharges, such as DC or radio-frequency capacitively coupled discharges, by the sputtering of a graphite cathode (Arnas *et al.*, 2010; Michau *et al.*, 2016a; Novikov *et al.*, 2021; Wang *et al.* 2020). This leads to the emission of a significant quantity of carbon, most of which is in the form of carbon-atom, C_2-dimer and possibly C_3-trimer (Bernholc and Phillips, 1986; Dominique and Arnas, 2007). The interaction of these injected primary species with active plasma species such as electrons, ions and radicals, leads to a molecular growth giving rise to large clusters (Michau *et al.*, 2016b). The identification and control of the nanostructures that can form in such situations require a detailed analysis of the molecular growth processes.

Despite their large number, experimental studies of the key-reactions involved in large clusters formation in plasma did not always make it possible to determine the structure, morphology, physical properties and molecular growth mechanisms. For this rea-

son, several groups made use of molecular simulation approaches. Most of the studies on carbon clusters were devoted to fullerenes and addressed more specifically the issues related to the thermal stability of this type of clusters. Among these studies, only very few made use of first principle simulations. This is for example the case of Celaya *et al.* (2017) who combined density functional theory (DFT) and quantum molecular dynamics simulations to study the thermal stability of quasi-fullerenes C_n (n = 20, 42, 48 and 60) at high temperature (800–1000 K). Actually, most of the computational studies on intermediate and large carbon clusters made use of molecular dynamics simulations with the Second-generation Reactive Empirical Bond Order (SREBO) potential to describe carbon-carbon interaction (Cai *et al.*, 2005; Kosimov *et al.*, 2010; Ueno and Saito, 2008). For instance, Zhang *et al.* (2005) used MD simulations with SREBO to study the thermal stability of four fullerene structures, i.e. C_{20}, C_{26}, C_{36}, and C_{60}. There are however only few investigations carried out on the reaction-mechanism involved in the formation of carbon clusters. Actually, the published studies dealt with fairly specific growth processes. For instance, Yamaguchi and Maruyama (1998) used molecular dynamics to study the formation of carbon clusters by the condensation of an atomic carbon vapor emitted by a graphite cathode. They showed that, in the temperature range 2500–3000 K and under a fairly high carbon-atom density, i. e., around 10^{19} cm^{-3}, the process starts with the formation of carbon dimers that grow and form linear then poly-cyclic molecules. If their density is high enough, these later undergo a coalescence process that results in different types of structures depending on the temperature level. More specifically, they observed that graphene-like structures are formed at temperatures below 2500 K, while fullerenes are obtained between 2500 and 3000 K. Molecular dynamics simulation studies similar to the example briefly described above mainly dealt with cluster formation by condensation in fairly dense carbon vapor where second order cluster-cluster reaction processes are very likely. There are however many situations where the formation of large carbon cluster proceeds by successive addition of carbon atoms or carbon dimers. This is especially the case in DC and RF glow discharges where carbon atoms and dimers produced by sputtering from a graphite electrode show much larger populations than the larger carbon clusters (Bernholc and Phillips, 1986). There is to our best knowledge only one study by Alekseev and Dyuzhev (1999) who investigated the formation of fullerene from polycyclic carbon structures. They made use of geometrical considerations to show that fullerene formation route from polycyclic clusters can take place by addition of a C_2-dimer. These authors focused however on a single growth route and did not give any qualitative or quantitative information on the reaction mechanism and on the probability of the growth process.

In spite of the lack of information and quantitative data on carbon cluster growth by addition of C-atom or C_2-dimer, several authors spent an important effort for developing kinetic models in order to understand carbon cluster formation in glow discharges, where the molecular growth process is dominated by C and C_2 addition (Michau *et al.*, 2016a; Schwiegert *et al.*, 1995). The implementation of these models faces a major difficulty related to the poor knowledge of the cross-section data for the collisions between carbon-atom or carbon-dimer and larger size carbon clusters. Some authors relied on approximate empirical expressions for the reaction rate constants (Michau *et al.*, 2016b), while others derived the reaction constants directly from the kinetic theory of gases. For this purpose, they used the apparent diameters of the clusters involved and assumed a value of 1 for the sticking probability of a carbon atom or dimer on larger carbon cluster (Schwiegert *et al.*, 1995).

Such an assumption is probably too much strong. Indeed, the possibility of non-reactive elastic or inelastic scattering cannot be disregarded. Moreover, the interaction dynamics and the sticking probabilities of C or C_2 with large carbon clusters are likely to significantly depend on the collision-energy and on the cluster size. Also, to our best knowledge, the structures and stability of the clusters resulting from the sticking process have never been studied in the literature.

The objective of this paper is related to this last point. Our aim is to investigate the growth of one intermediate, i.e. C_{36}, and one large, i.e. C_{80}, fullerenes by C-atom addition. We are particularly interested in examining the possibility to preserve the fullerene structure during the growth process or to recover this structure by an annealing of the reaction product. The choice of C_{36} was motivated by the fact that fullerene isomers show significant stability and abundance under the conditions of interest only for clusters with more than 32 atoms (Allouch *et al.*, 2021). C_{80} was considered in order to investigate how the cluster size affects the sticking mechanism and probability. We make use of classical molecular dynamics to analyze the interaction of carbon-atom with the fullerenes considered, to identify the different sticking configurations and to investigate their stabilization by annealing. We determine the partial sticking probability for each configuration and infer the overall sticking cross-sections as function of the collision energy. Two simulation sets using two bond-order interaction potentials optimized for C–H system were used. The first one, SREBO, takes into account only short range interactions while the second, Adaptive Intermolecular Reactive Empirical Bond Order (AIREBO), takes into account torsional effects and long range interactions.

The paper is organized as follows. In the Sec. II we briefly give the main feature of our MD approach and discuss the methodology adopted to determine the sticking probabilities and cross sections for C-atom/Fullerene interactions. The set up of our simulation is presented in Sec. III. In Sec. IV, the simulation results obtained using SREBO and AIREBO are discussed. The different sticking configurations along with their probabilities as function of the collision-energy are analyzed. The total sticking probabilities and cross-sections are then inferred from this analysis.

II. MODELING AND SIMULATION METHODOLOGY

The determination of the sticking cross-section on a 3D cluster for a prescribed collision energy, i.e., a projectile velocity magnitude in the target cluster frame, requires calculating the average sticking probability over a large number of projectiles arriving from all space directions with randomly oriented velocity. For this purpose and in the case of fullerene clusters that usually show quasi-spherical geometry, we define a reference sphere, also called interaction sphere (S_{int}), centered at the cluster center of gravity and with a radius R_{int} (cf. 1). This radius depends on the maximum distance d_{max} separating two atoms in the cluster structure (i.e. the diameter in the case of a spherical fullerene) and on the cut-off radius R_{cut} of the interaction potential following the expression (Ning *et al.*, 2017):

$$R_{\text{int}} = 2.2\left(\frac{d_{\max}}{2} + R_{cut}\right) \quad (1)$$

The cut-off radius R_{cut} are set to 2 and 3 Å for the SREBO potential and for the short range interactions in AIREBO potential, respectively (Stuart *et al.*, 2000). The estimated values of d_{max} are 6 Å and 10 Å, for C_{36} and C_{80}, respectively. The radius of the interaction sphere is chosen so as: i - the target and the projectile do not interact when starting the simulation when the projectile atom is located on the interaction sphere ($R_{int} > R_{cut} + \frac{d_{max}}{2}$); and ii - the initial distance between the projectile and the target is greater than the distance between two atoms of the target, $R_{int} > d_{max}$. Equation (1) enables R_{int} fulfilling both conditions. In fact, one can make use of any R_{int} value greater than the one given by Eq. (1). However, a too large value of R_{int} makes it necessary to perform a large set of simulations when investigating the effect of the angle and requires longer computation time for each simulation. The factor 2.2 enables satisfying the conditions mentioned above while keeping reasonable computation time.

If a large number of projectile C-atom with initial positions randomly distributed on the interaction sphere are sequentially submitted to the target cluster with a prescribed velocity magnitude and a randomly distributed velocity direction, the average sticking probability at the collision-energy, ε_{col}, corresponding to the prescribed velocity magnitude depends on the fraction of the atoms that stick to the cluster and is given by Eq. (2):

$$\langle p_{sticking} \rangle = \frac{N_{stuck\ atoms}}{N_{total\ atoms}} \tag{2}$$

where N_{stuck} and N_{total} denote the number of atoms that stick to the cluster and the total number of atoms used in the simulation, i.e. the total number of trajectories, respectively.

The number of sticking events experienced by a given target cluster during Δt is given by the following rate equation:

$$N_{stuck\ atoms} = \sigma \times \nu^* \times n_{pro\ jectile} \times \Delta t \tag{3}$$

where $n_{pro\ jectile}$ is the density of the projectile atom, σ the cross-section assumed constant for the sake of simplicity in this derivation and $\nu^* = \sqrt{\frac{8k_BT}{\pi m}}$ the thermal velocity of the projectile. Actually, $\sigma \times \nu^*$ represents the sticking rate.

The expression of $N_{stuck\ atoms}$ maybe also rearranged:

$$N_{stuck\ atoms} = \left(S_{\text{int}} \times \nu^* \times \frac{n_{projectile}}{4} \times \Delta t \right) \times \frac{4 \times \sigma}{S_{\text{int}}} \tag{4}$$

The factor in brackets represents the number of projectiles entering the interaction sphere during Δt, referred to as $N_{pro\ jectile}$, provided the interaction potential is negligible with respect to the projectile kinetic energy for a length-scale of the order of the interaction sphere diameter, which is the case here as will be discussed below.

The sticking cross-section $\sigma_{sticking}(\varepsilon_{col})$ may be therefore expressed as a function of the average sticking probability $\langle p_{sticking} \rangle$ and of the cross-sectional area of the interaction sphere, $S_{\text{int}} = \pi R_{\text{int}}^2$, as follows:

$$\sigma_{sticking}(\varepsilon_{col}) = \langle p_{sticking} \rangle \times S_{\text{int}} \tag{5}$$

It is worthy to mention at this stage that the cross-section value determined from Eq. (5) does not depend on the surface of the interaction sphere. Actually, the quantity that depends on the surface of the interaction sphere is $\langle p_{sticking} \rangle$, and, for a given collision-energy, $\langle p_{sticking} \rangle$ varies linearly with the surface of the interaction sphere so as the sticking cross-section remains constant.

Also noteworthy is the fact that the cross-section values that can be determined using the above approach cannot exceed the cross-sectional area of the interaction sphere. As a matter of fact, the sticking cross-section is given by the product of the sticking probability ($\langle p_{sticking} \rangle < 1$) and the cross-sectional area of the interaction sphere. This means that our methodology is only valid for collision-energy values where the cross-section is below the cross-sectional area of the interaction sphere. We have therefore to make sure that this is the case in the investigated range of collision-energy. The potential energy values of the interaction between the projectile at its initial position on the interaction sphere and the closest target atom, i.e., for C–C distances of 10.2 and 13 Å in the cases of C_{36} and C_{80}, respectively, are below 1.5×10^{-5} and 3.6×10^{-6} eV. Therefore, for the collision-energy range investigated in this study, i.e., 5×10^{-3} eV $< \varepsilon_{col} <$ 20 eV, the projectile does almost not interact with the target outside the interaction sphere (the potential energy is too small compared to the kinetic energy). Consequently, the projectiles with energy values in the range considered in this study and impact parameters greater than the radius of the interaction sphere cannot be attracted towards the target clusters. This means that the sticking cross-section is necessarily smaller than the cross-sectional area of the interaction sphere in the investigated range of the collision energy. This validity condition is therefore fulfilled.

The calculation of the sticking cross-section requires the determination of the average sticking-probability over a carbon-atom population crossing the interaction sphere toward the target cluster. This was carried out using a two-step procedure:

The first step involves the uniform distribution of a large number of projectile atoms on the surface of the interaction sphere. This is performed using two random numbers η and ε uniformly distributed in [0, 1] to sample the cosine of the angle θ_s and the angle φ_s that determine the position of the projectile atom on the interaction sphere (cf. Fig. 1).

In the second step, we sample for each projectile atom the incidence direction defined by the set of angles θ_v between the velocity vector and the normal to the interaction sphere and φ_v the azimuthal angle in the plane that is tangent to the interaction sphere at the initial position of the projectile atom (cf. Fig. 1). The sampling procedure is similar to the one used for θ_s and φ_s.

The second step enables averaging the sticking probability over the different velocity directions for each projectile, while the first step enables averaging the sticking probability over the surface of the interaction sphere crossed by the projectiles coming from all space-directions. Note that the above procedure is fully equivalent to averaging the sticking probability over the impact positions and angles on the cluster surface. Also, the two steps involved in the procedure can be carried out independently, i.e. in any order.

Exploring all the trajectories in this four-dimensional variable-space, (θ_s, φ_s, θ_v, φ_v) without any simplification can be extremely costly in terms of computation time. A simplified step-by-step procedure was therefore used to determine the impact of each collision parameter on the sticking probability so as to take into account only

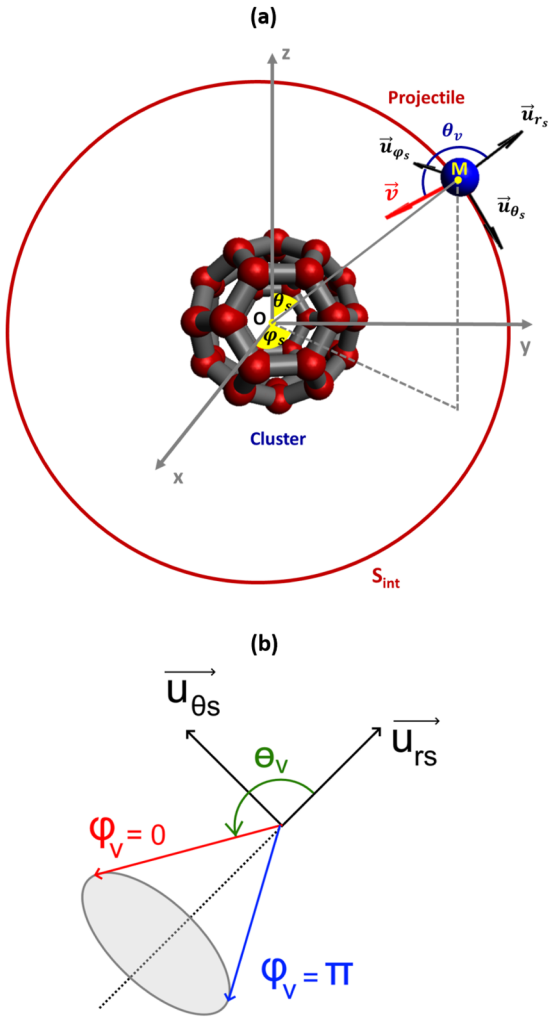

FIG. 1. (a) Schematic of the interaction sphere S_{int} with the target cluster positioned at the center and the projectile at the initial position of the trajectory on the surface S_{int}. (b) Details view emphasizing the angles θ_v and φ_v that define the initial velocity vector of the projectile.

the most important ones in the final estimation of the overall sticking probability and cross-section.

We first start by randomly positioning a large number of projectiles on the surface of the interaction sphere, i.e. we first sample θ_s and φ_s. Then, we investigate the variation of the average sticking probability over all the interaction sphere as a function of the projectile velocity magnitude for a velocity direction perpendicular to the interaction sphere. This means that we average the sticking probability over the angles θ_s and φ_s for $\boldsymbol{\theta_v = \pi}$ and for a collision energy ε_{col}. Since this probability corresponds to $\theta_v = \pi$, it does not depend on the azimuthal angle φ_v. The average will be therefore denoted $\langle p_{sticking} \rangle_{\theta_s,\varphi_s}(\varepsilon_{col}, \theta_v = \pi)$. The aim of this first step is not only to have a first estimate of the sticking probability, but also to investigate the sticking mechanism and the resulting sticking configurations.

Then, we investigate the effect of the projectile velocity direction and more specifically the angle θ_v. For this purpose, we perform MD simulations for 13 values of $\cos(\theta_v)$, uniformly distributed between −1 and 0, four values of the collision energy ε_{col}, and two values of the angle φ_v, i.e. 0 and π on the 2000 projectile atoms randomly distributed on the surface of the interaction sphere. The impact of the angle φ_v was eventually studied for each initial position of the projectile.

III. SIMULATION PROCEDURE

A. Interaction potential

We employed two reactive bond order potentials, namely the second generation of the REBO potential called SREBO (Brenner *et al.*, 2002) and the adaptive intermolecular REBO referred to as AIREBO (Stuart *et al.*, 2000), to characterize the interaction between carbon atoms. Using the Tersoff bond-order formalism, these potentials provide precise handling of covalent-bonding reactions and are specifically parameterized for carbon and hydrocarbon systems.

The first potential (SREBO) is the simplest one. It provides a good empirical description of covalent bonds for non-polar systems and has been widely used in the literature for studying the stability and structural properties of many carbon systems, including fullerenes and graphenes (Cai *et al.*, 2005; Kosimov *et al.*, 2010; Lai *et al.*, 2017). The results obtained using SREBO are comparable to those obtained theoretically by DFT (Jones, 1999). This potential was also used to study cluster-surface or cluster-cluster interactions. For instance, Dzhurakhalov *et al.* and Ulukmuradov *et al.* used it to examine the interaction between ring-shaped carbon clusters and a rectangular nanographene (Dzhurakhalov *et al.*, 2015) as well as the adsorption of C_{60} fullerene onto the surface and at the edges of defect-free graphene (Ulukmuradov *et al.*, 2021), respectively. The SREBO expression and parameters used in our calculation can be found in (Brenner *et al.*, 2002).

Despite its effectiveness in describing the carbon-carbon covalent bond, SREBO potential suffers from certain limitations, namely the lack of long range interactions between non-bonded atoms and the inability to depict rotational degree of freedom around single C–C bonds due to the absence of torsional interactions.

To overcome these shortcomings, Stuart *et al.* (2000) developed the adaptive intermolecular REBO potential (AIREBO) that incorporates the Lennard-Jones potential to account for non-bonded interactions and a novel torsional energy expression to describe rotation around single C–C bonds. Surprisingly, there are only very few investigations that make use of molecular dynamics simulations with AIREBO potential. These are essentially devoted to fullerene-fullerene and fullerene-graphene interactions and coagulations (Hosseini-Hashemi *et al.*, 2018; Rysaeva *et al.*, 2018).

B. Simulation steps and parameters

Our simulation procedure starts by generating a stable carbon-cluster at a temperature of 0 K at the center of a 100 × 100 × 100 $Å^3$ simulation box. This is performed by the combined condensation-annealing (CCA) method described in details in (Allouch *et al.*, 2021). In this method, the abundance of the different cluster structures for a cluster size n, is determined statistically by submitting n

carbon atoms initially at 0 K and randomly positioned in a simulation box to an annealing process that involves a heating phase up to a prescribed maximum temperature, a rest phase at this temperature and a cooling phase down to 0 K. This process usually starts with the condensation of the carbon cloud under the action of the attractive forces between the initially free carbon atoms at the early stage of the heating phase. This condensation ends up with the formation of a carbon cluster that undergo several rearrangements during the annealing process (Allouch *et al.*, 2021). Extensive parametric investigation were carried out in order to determine the set of values for the duration of the heating, cooling and rest phases, and the temperature during the rest phase that enables determining the most stable structure. These are 100, 100 ns, 100 ps and 3000 K, respectively (Allouch *et al.*, 2021).

For C_{36}, the isomer used in our study is the one that has the lowest potential energy with a value of −6.68 eV/atoms, which is in close agreement with the most stable isomer obtained with Basin-Hopping method (Lai *et al.*, 2017) and with time going-backwards (TGB) technique (Gao *et al.*, 2007). In the case of C_{80}, the isomer used in our study has an elliptic shape with an energy equal to −7.21 eV/atoms and a bond-length distribution in the range 140–150 pm, which is in good agreement with the most stable C_{80} isomer (E = −7.29 eV/atom, bonds lengths: 140–146 pm) obtained by (Furche and Ahlrichs, 2001) using DFT.

Prior to the simulation of its interaction with a carbon atom, a cluster obtained by the CCA method described above is first heated to 300 K during 10 ns using Berendsen's thermostat (Sharma *et al.*, 2019) with a thermal relaxation time of 1 fs. It is then kept at a temperature of 300 K for 0.01 ns using the same thermostat. After the equilibration of the cluster positioned at the center of the simulation box, a carbon atom (the projectile) is sampled and submitted toward the cluster. The simulation was performed in the micro-canonical NVE ensemble (NVE: number of particles N, volume V, and energy E are constant) and the integration time-step was set to 0.1 fs. The simulation is stopped after three times the duration necessary to cross the interaction sphere. This time-limit was determined after an extensive analysis. On one hand, it is short enough to avoid the exit from the simulation box of projectiles that do not stick to the target and exit the interaction sphere, thus enabling to identify reflection or insufficient contact (no sticking) events. On the other hand, it is long enough to enables full relaxation after sticking processes and thus to identify not only sticking events but also the different configurations that may be obtained.

In order to determine the optimal number of trajectories needed to achieve statistically significant sticking probabilities, we performed several sets of 2000 trajectory simulations of C–C_{80} collision for representative values of the collision energy between 5.24 meV and 0.21 eV (see results in supplementary materials). The simulation required an average execution time of 33 central processing unit (CPU) hours per run on our computing cluster. A good trade-off between computation cost and statistically significant sticking probability values is obtained with 600 trajectory simulations in the investigated range of collision-energy.

Carbon cluster elaboration environments, such as non-equilibrium plasmas or thermal arcs, usually contain fast ions or neutrals that carry a significant amount of energy, i.e., between few tenths of eVs and few eVs, along with a much colder background gas (Dominique and Arnas, 2007; Farhat and Scott, 2006; Michau *et al.*, 2016b). Therefore, it is very likely that the structures resulting from the sticking processes undergo collisions with these high-energy species and gain a significant amount of energy, i.e., excitation of the internal, electronic, vibrational or rotational, modes or heating of the translational mode. This excitation/heating phase is subsequently followed by a relaxation phase due to the collisions of the sticking products with the much colder background gas molecules. This collisional heating/relaxation process may lead to a significant structural change. Consequently, the ultimate structure of the produced cluster depends not only on the sticking mechanisms, but also on the subsequent collisional relaxation. This collisional heating/relaxation process is of course very complex and its detailed investigation is beyond the scope of the present study. However, a first analysis of the consequence of this process on the structure of the sticking product may be performed using a simulated annealing where the excitation phase is described by a temperature increase of the sticking product while the relaxation phase is simulated by a thermal quenching. This was performed using the molecular dynamics approach described in (Allouch *et al.*, 2021). The annealing cycle involves 100 ns heating phase up to 2000 K, 100 ns rest phase at 2000 K and 10 ns cooling phase down to 0 K. The initial temperature of the cycle is in the range 300–1000 K. It corresponds to the temperature of the produced C_{n+1} cluster at the end of the sticking process which depends on the C-C_n collision energy.

IV. RESULTS AND DISCUSSION

A. Typical sticking configurations

The simulations showed that the collisions between C-atom and the fullerene may result either in an elastic scattering, an inelastic scattering or a sticking with the formation of a larger carbon cluster. No cluster fragmentation was observed in the investigated range of collision-energy. In the following, we do not distinguish between the elastic and inelastic scatterings. As for sticking, the coordination number analysis using MD simulations showed the existence of four sticking configurations (Fig. 2). In the first configuration, the projectile atom remains on the surface of the fullerene and is bound to only one atom of the target cluster [Fig. 2(a)]. This sticking configuration, referred to as surface-sticking, dominates at low collision energy. The other three sticking configurations lead to the formation of a carbon cluster, where the projectile atom is embedded in the core of the cluster. The three sticking configurations belonging to this second category differ by the number of the target cluster atoms that bind to the projectile atom after the collision. We may have two-, three- or four-neighbor configurations denoted 2N-, 3N-, and 4N- sticking configurations, respectively. These are depicted in Figs. 2(b)–2(d), respectively.

In principle, classical molecular dynamics does not allow a direct characterization of the hybridization state of the atom. This need considering orbital overlap and is therefore based on a quantum approach. Here, we are using a bond-order method where each C–C bond is characterized by its order that is determined by its length and the angles with the adjacent bonds. In the case of the 2N-sticking configuration, the projectile establishes two bonds of 1.43 Å, which is intermediate between the length-values of simple (1.54 Å) and double (1.33 Å) C–C bonds and would therefore correspond to conjugated bonds as thoroughly discussed by Brenner (Brenner *et al.*, 2002; Brenner, 1990) in the frame of the bond-order

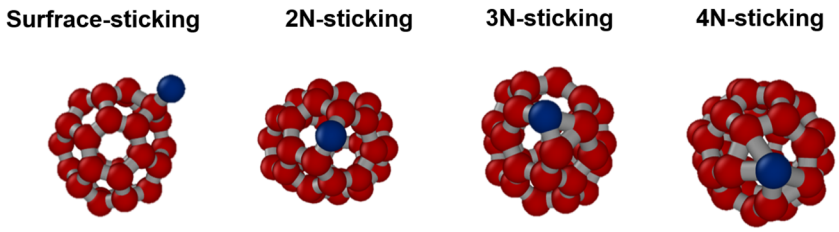

FIG. 2. Illustration of the different types of sticking configuration resulting from C–C_{36} interaction. The atom in blue is the projectile atom.

approach. In the case of the 3N-sticking configuration, the projectile establishes three bonds of 1.36, 1.56 and 1.49 Å, which approximately corresponds to one double bond, one single bonds and a bond that is intermediate between a single and double bond, respectively. Although it is difficult to conclude, the projectile atom seams not far from a sp^2 hybridization.

B. Sticking configurations probabilities as function of the collision energy

The variation of the probabilities $\langle p_{sticking}\rangle_{\theta_s,\varphi_s}(\varepsilon_{col},\theta_v=\pi)$ for the different sticking configurations as function of the collision energy for C_{36} are shown in Fig. 3(a) for SREBO potential and Fig. 3(b) for AIREBO.

When using SREBO potential, i.e. in the absence of long-distance interactions and torsional effects, the surface-sticking configuration is strongly dominant for collision-energy below 2.50 eV. This value corresponds to the C–C binding energy in the fullerene structure. The predominance of the surface sticking configuration in this case can be simply explained by the fact that the incident atom does not have enough energy to break a C–C bond of the target and to establish new bonds with two or more neighbors. When increasing the projectile energy, the surface-sticking probability decreases almost exponentially from a value of ~0.9 at very low energy to less than 0.1 at 20 eV. The 2N-sticking configuration in which carbon atom is embeded in the target fullerene structure takes over from the surface-sticking at a collision-energy of 2.50 eV. The corresponding probability reaches a maximum value ~0.55 at 7 eV. Beyond this energy, the probability of 2N-sticking configuration decreases and the 3N-sticking configuration takes over and becomes dominant beyond 15 eV. Its probability increases almost linearly with collision energy and reaches a value of 0.5 at 20 eV. The sticking with four neighbors remains very minor in the energy range studied.

The variations of the sticking probabilities $\langle p_{sticking}\rangle_{\theta_s,\varphi_s}(\varepsilon_{col},\theta_v=\pi)$ with the collision-energy obtained with AIREBO potential are depicted in Fig. 3(b). These show significant differences as compared with those obtained with SREBO. First, the activation of the processes leading to 2N- and 3N-sticking configurations requires a much larger energy. For example, sticking to two neighbors requires an activation energy of 2 eV with AIREBO, while it shows significant probability even for a collision-energy value as low as 0.58 meV with SREBO. As for the surface-sticking configurations, SREBO results in a monotonous and regular decrease of the sticking probability that reaches almost zero at 20 eV, While AIREBO leads to a much less regular variation. One may distinguish two energy domains. A first one below 2.5 eV

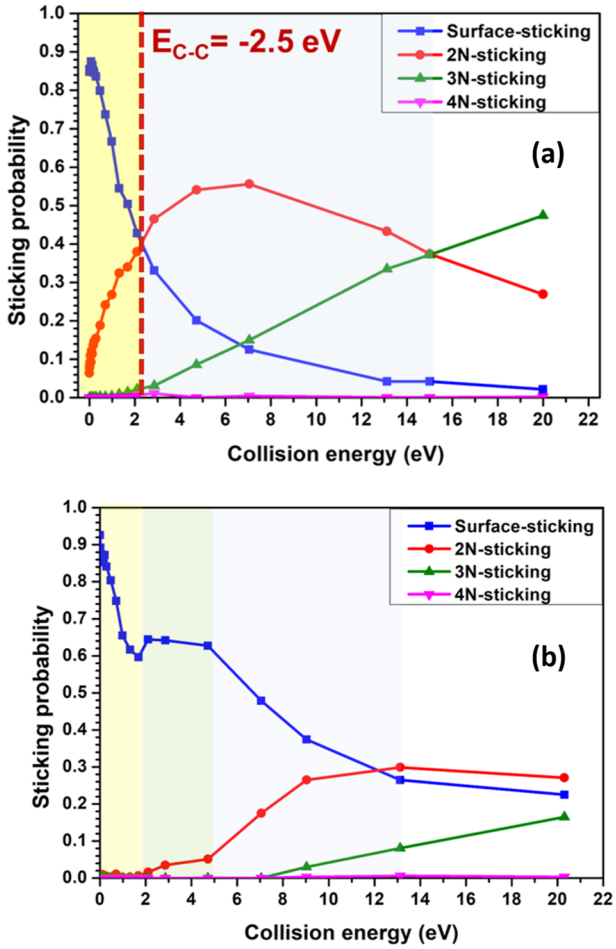

FIG. 3. Sticking probabilities of the different sticking-configurations as function of the collision energy for C_{36} fullerene calculated using SREBO (a) and AIREBO (b) potentials.

with probability variation trend similar to the one obtained with SREBO, and a second one above 2.5 eV with a much slowly varying probability and a significant probability value even at high energy. This significant difference is due to the difference between the sticking mechanisms obtained for each potentials.

These mechanisms are discussed in the Sec. IV C.

C. Sticking reaction and collisional relaxation mechanisms

1. Surface-sticking configuration

The first mechanism that dominates at very low collision-energy leads to a sticking configuration, where the projectile atom stays at the surface of the target fullerene. When SREBO potential is used, this mechanism does not involve any bond breaking or reconstruction in the bulk structure of the target fullerene. The carbon atoms surrounding the reaction site are nevertheless stabilized by the sticking process, as shown in Fig. 4. An annealing at 2000 K leads to the incorporation of the carbon atom into the fullerene structure (cf. Fig. 5). As a result, a more stable fullerene like structure with an additional carbon atom is formed.

When using AIREBO potential, the analysis of the different mechanisms that lead to a surface sticking configuration shows the existence of two collision-energy domains. For a collision energy below 2 eV, the sticking mechanism is similar to the one observed with SREBO potential and discussed previously. Above 2 eV, the surface-sticking configuration may result from several reaction routes. The most significant ones are illustrated in (Fig. 6). This shows a first case where the interaction between the projectile atom and the fullerene involves a first step where the projectile sticks to two neighbors [Fig. 6(a)]. The intermediate complex is not stable enough and one of the bonds formed in the first step is broken, which ends up with a surface sticking configurations. A second mechanism shown in Fig. 6(b) involves a first step where the projectile sticks to a single neighbor, followed by a second step where the sticking site is substituted by another one while always keeping a surface sticking configuration [Fig. 6(b)]. Eventually, a third example is depicted in Fig. 6(c) where the projectile sticks to two neighbors in a first step. Then, a structural rearrangement of the cluster ends up with a surface-sticking configuration and the subsequent formation of a heptagonal defect in the bulk structure of the cluster.

2. 2N-sticking configuration

The process leading to 2N-sticking configuration involves a C–C bond breaking in the bulk structure of the target cluster. This bond is shared either between two hexagons, one hexagon and one pentagon, or, to a much lesser extent, two pentagons. Figure 7 shows the reaction dynamics for the three sticking mechanisms mentioned above. When the projectile atom (k) breaks the bond i–j shared between a pentagon and a hexagon, the sticking dynamics starts by a first phase where the projectile atom (k) establishes a bond (k–i) with a single neighbor (i). This leads to the formation of a highly unstable transition state with a nine-atom cycle [Fig. 7(a-2)]. Then, in a second phase, the projectile establishes a bond (k–j) with the second atom (j) of the broken bond (i–j). As a result, a fullerene-like structure with a heptagon-hexagon defect is obtained [Fig. 7(a-3)]. This defect may be readily eliminated and transformed to a hexagon pair

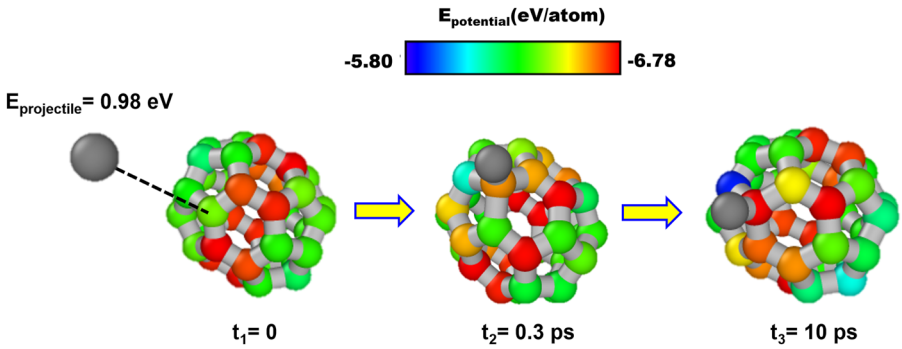

FIG. 4. Effect of the surface-sticking process on the stability of the target fullerene in the case of C_{36} and SREBO potential. One can notice that the potential energy of the atoms surrounding the sticking site show substantial decrease after the sticking process, which indicates a significant stabilization.

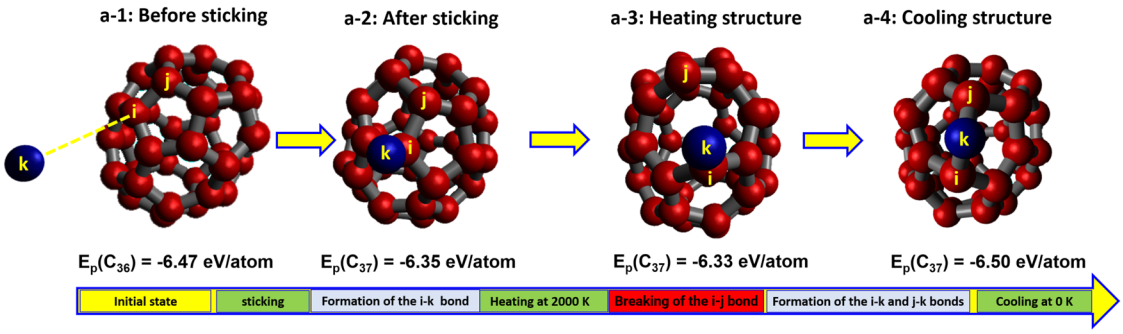

FIG. 5. C_{36} interaction leading to surface-sticking configuration and incorporation of the carbon atom into the C_{36} fullerene structure after annealing. The simulation was performed with SREBO potential.

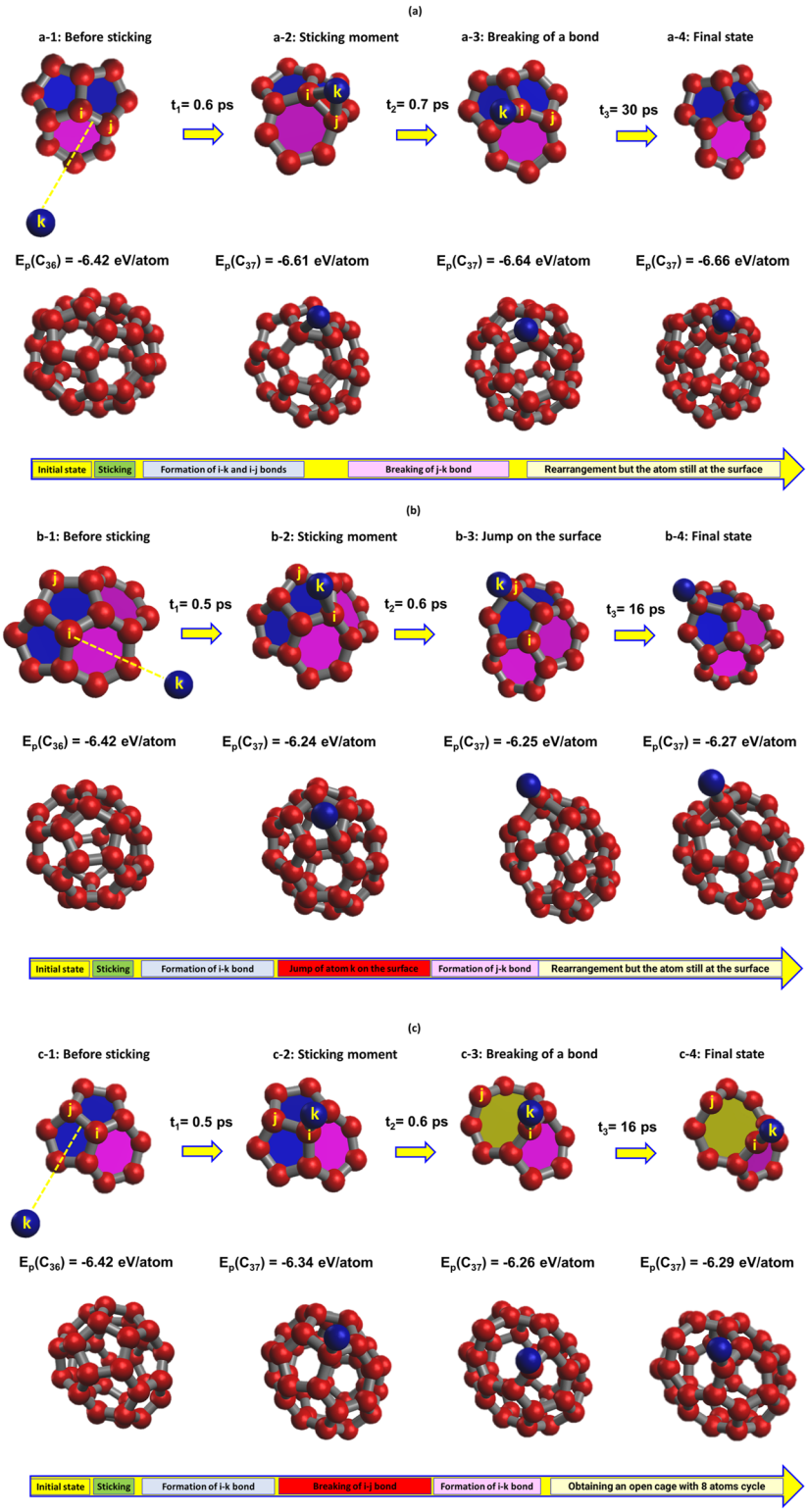

FIG. 6. Different C_{36} interaction mechanisms leading to a surface-sticking configuration with AIREBO potential. For each mechanisms (a), (b) and (c) the first row enables identifying the reaction site and the nature of the cycles involved in the process, while the second row shows the overall transformation of the cluster. The potential energy in eV/atom for the involved cluster structures are indicated.

after a simulated annealing at a temperature of 2000 K as shown in Fig. 7(a-4).

When the projectile atom breaks a pentagon-hexagon shared bond (i–j), the sticking process starts by a first phase where the projectile atom (k) establishes two bonds, denoted (k–i) and (k–j) [cf. Fig. 7(b-2)], with two neighbors (i and j). This leads to the formation of a transition state with two heptagon cycles [cf. Fig. 7(b-2)]. This structure relaxes without any rearrangement. As a result, a fullerene like structure with a heptagon-heptagon defect is obtained [Fig. 7(b-3)]. A simulated annealing at 2000 K eliminates one of these heptagons by transforming a pentagon-heptagon pair into a hexagon pair as shown in Fig. 7(b-4).

When the projectile atom breaks a pentagon-pentagon shared bond (i–j), cf. Fig. 7(c-2), the sticking process starts by a first phase where the projectile atom (k) establishes a bond with a single neighbor (i), denoted k–i. This leads to the formation of a highly unstable transition state with eight-atom cycle. Then, in a second phase, the projectile establishes a second bond with the second atom (j) of the broken fullerene bond. The formation of k–j bond leads to the transition from eight-atom cycle to two hexagonal cycles [Fig. 7(c-3)]. The annealing of this structure, at 2000 K, results in transforming the two hexagons into a pentagon-heptagon pair. As a result, a fullerene with a heptagonal defect is obtained as shown in Fig. 7(c-4).

3. 3N-sticking configuration

The 3N-sticking configuration is obtained in two situations corresponding to trajectories where the collision takes place at the center of a pentagon or a hexagon, as shown in Fig. 8. When the collision takes place at the center of a pentagon, the sticking mechanism starts by a first phase where the projectile atom establishes three bonds with three neighbors, which leads to the formation of a highly unstable transition state with a three-atom cycle and a heptagon [Fig. 8(a-2)]. This structure relaxes without undergoing any rearrangement. As a result, a fullerene like structure with two defects is obtained [Fig. 8(a-3)]. The triangle-pentagon defect linked to the three-atom cycle can be eliminated and transformed to a hexagon after a simulated annealing at a temperature of 2000 K as shown in Fig. 8(a-4).

When the collision takes place at the center of a hexagon, the sticking process starts by the formation of four bonds with four neighbors, which results in a highly unstable transition state with a triangle-triangle pair [Fig. 8(b-2)]. One of these triangles is eliminated by the conversion of a triangle-pentagon pair to a hexagon. As a result, a fullerene like structure with a triangle defect is obtained [Fig. 8(b-3)]. This defect is eliminated and transformed to a hexagon after a simulated annealing at a temperature of 2000 K as shown in Fig. 8(b-4).

D. Overall sticking probability of carbon atom on a C_{36} and C_{80} fullerenes

We discuss, first, the variation of the sticking probability as a function of the collision energy for situations where the projectile is directed toward the center of the cluster, i.e. we discuss the variation of $\langle p_{sticking}\rangle_{\theta_s,\varphi_s}(\varepsilon_{col},\theta_v=\pi)$. Then, we investigate the variation of the sticking probability with θ_v and φ_v. The overall sticking cross-sections are then determined from these probabilities for C_{36} and C_{80} fullerenes.

1. Sticking probability as a function of the collision energy

We performed two sets of simulations, a first one with SREBO potential and a second one with AIREBO. The collision-energy range explored in the two sets is 0.58 meV–20 eV. The results are shown in Fig. 9. The sticking probability obtained With SREBO remains high, and typically greater than 0.78 over the entire energy range considered. It shows significant variation over a limited energy range, i.e., 0.58 meV–2 eV, a pronounced maximum value of 1 at 0.2 eV and remains almost constant above 2 eV.

Figure 9 also shows the variation of the sticking probability with the collision energy obtained for C_{80} using SREBO. The results are similar to those obtained for C_{36}, except at very low energy, i.e., $E_{inc} < 0.2$ eV, where the sticking probability for C_{80} is much lower, with a value of 0.56 at 0.58 meV. This is due to the fact that the bonds between the carbon atoms in the C_{80} are much stronger, and larger collision energy is required in order to break a C–C bond in the C_{80} (cf. Fig. 10).

The variations of the sticking probabilities $\langle p_{sticking}\rangle_{\theta_s,\varphi_s}(\varepsilon_{col},\theta_v=\pi)$ with the collision energy determined with AIREBO potential show a very different behavior as compared to SREBO for both C_{36} and C_{80}. In particular, the two potentials yield opposite trends for these variations at low energy ($E_{inc} < 2$ eV). Indeed, the sticking probabilities calculated with AIREBO show significant decreases and pronounced minima at 2 eV approximately. At high collision energy, SREBO and AIREBO yield similar probability variation trends with almost constant values. However, AIREBO gives a significantly lower sticking probability for both C_{36} and C_{80}.

The large differences between the total sticking probability values obtained by SREBO and AIREBO are mainly due to the presence of the long range interaction Lennard-Jones (LJ) potential. This is shown in Fig. 11 where we depicted the sticking probability values as function of the collision energy obtained when either the LJ interaction term or the torsional energy term are taken into account or disregard. The figure shows that the sticking probabilities obtained by AIREBO when LJ term is disregarded are practically equal to those obtained using SREBO. Actually, the effect of these long range interactions is a further stabilization of the target cluster (cf. Fig. 10) with a subsequent decrease of the overall sticking probability.

The difference in the variation trends of the sticking probabilities as function of the collision-energy between SREBO and AIREBO is the consequence of the differences in the sticking mechanisms and in the values of the energy required to activate 2N- and 3N-sticking configurations.

When SREBO potential is used, the decrease of the probability for the surface-sticking configuration at very low energy ($E_{inc} < 0.2$ eV) is largely compensated by the significant increase of the probability for 2N-sticking configuration. This explains the net increase of the overall sticking probability at very low energy,

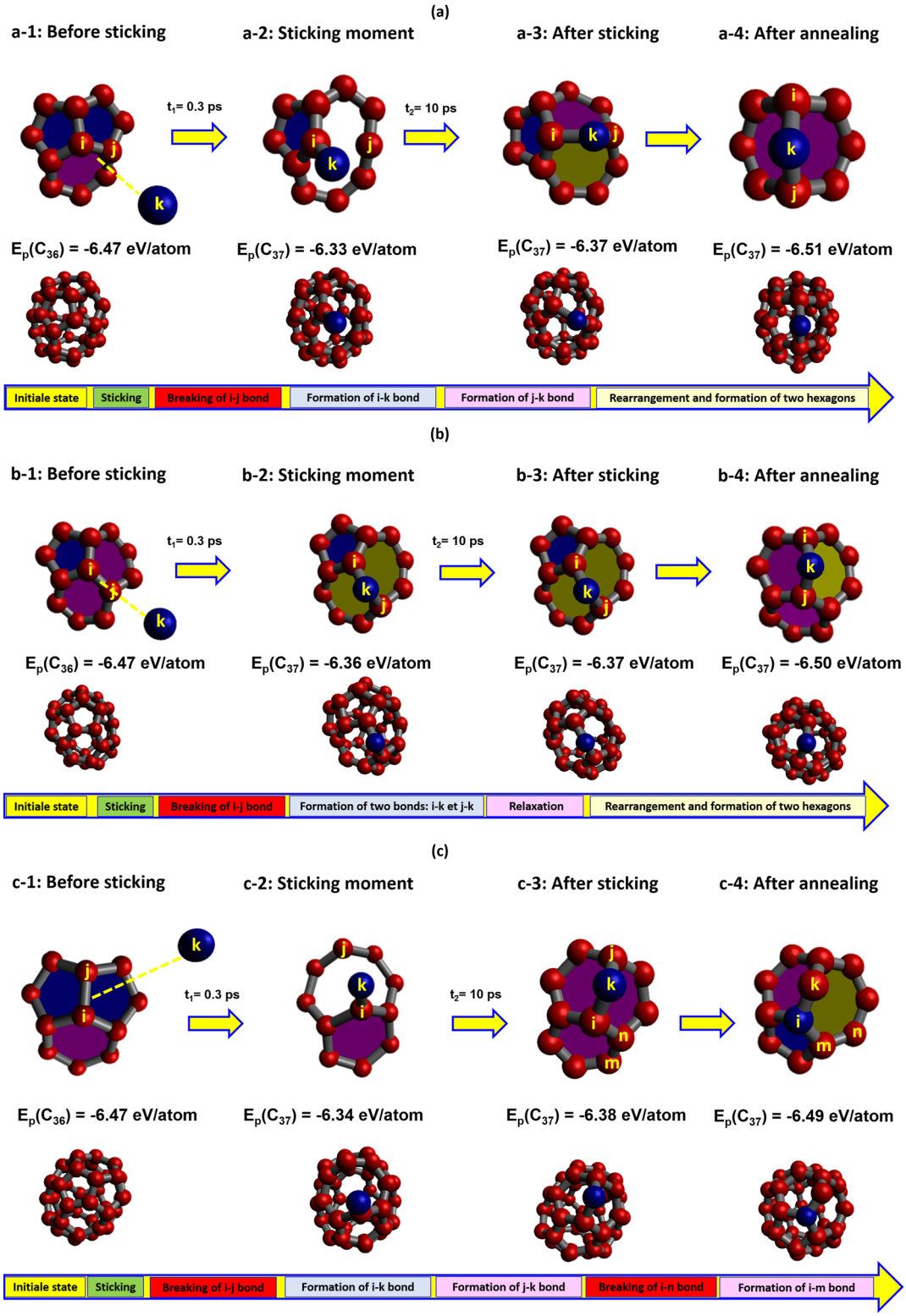

FIG. 7. Different C_{36} interaction mechanisms leading to 2N-sticking configuration with SREBO potential. For each mechanisms (a), (b) and (c) the first row enables identifying the reaction sites and the nature of the cycles involved in the process, while the second row shows the overall transformation of the cluster. The potential energy in eV/atom for the involved cluster structures are indicated.

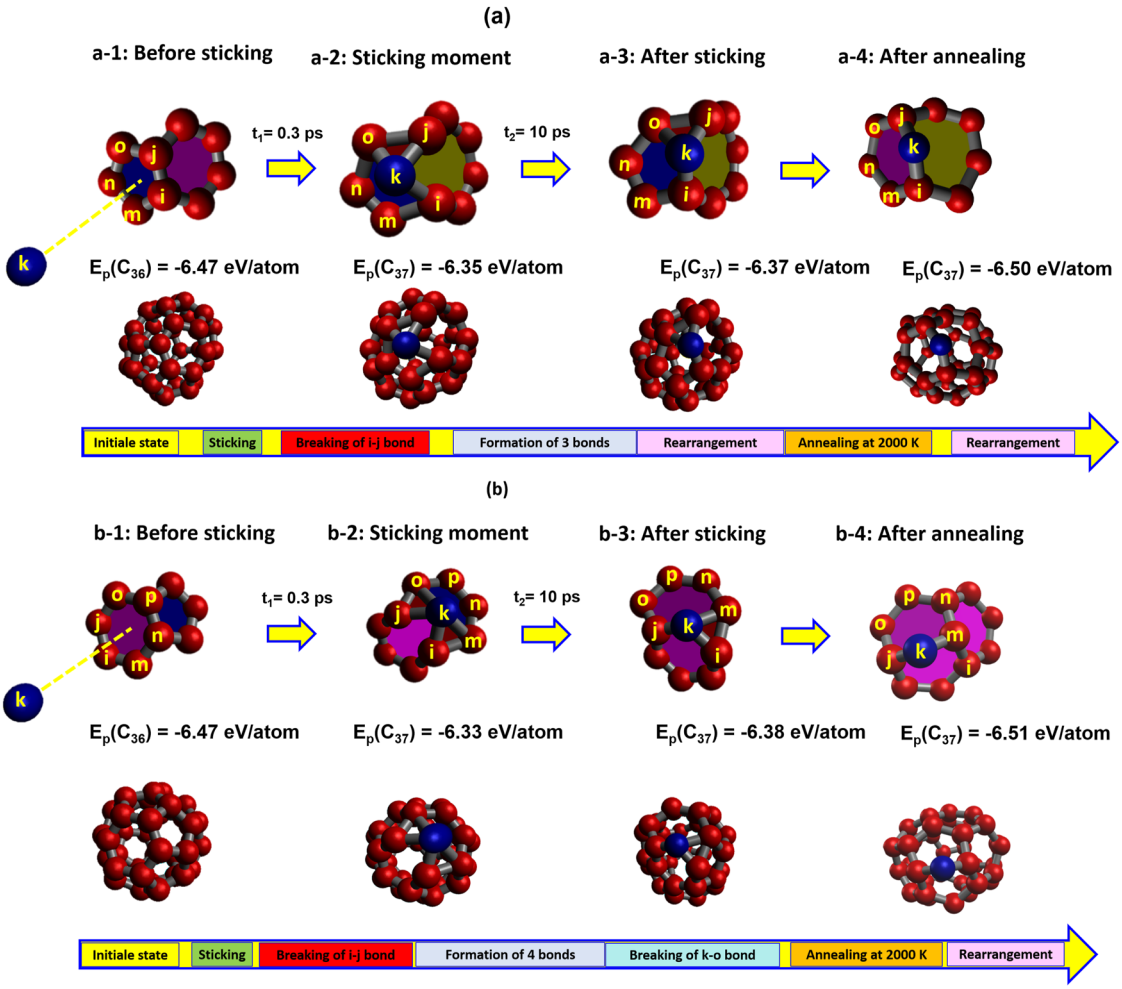

FIG. 8. Different C_{36} interaction mechanisms leading to a 3N-sticking configuration with SREBO potential. For each mechanisms (a) and (b) the first row enables identifying the reaction site and the nature of the cycles involved in the process, while the second row shows the overall transformation of the cluster. The potential energy in eV/atom for the involved cluster structures are indicated.

as discussed previously (cf. Fig. 3). At intermediate energy values (0.2 eV < E_{inc} < 2 eV), this compensation effect is no more effective and the overall sticking probability reaches a maximum and then decreases. In the case of AIREBO, the decrease of the probability for the surface-sticking configuration is not compensated by any other mechanism at very low energy. The 2N-sticking configuration is indeed active only above 2 eV and its probability shows very small value. This explains the net decrease of the overall sticking probability $\langle p_{sticking}\rangle_{\theta_s,\varphi_s}(\varepsilon_{col}, \theta_v = \pi)$, which shows opposite behavior as compared to the SREBO case. The occurrence of the surface-sticking configuration is enhanced by the activation of additional complex mechanisms when AIREBO is used (cf. Fig. 6). As a result, the corresponding probability reaches a minimum at a collision energy of 2 eV and then slightly increase.

The partial probabilities for the different sticking configurations show large variations at high collision-energy (cf. Fig. 3). Nevertheless, a compensation effect takes place between the different sticking channels and the overall sticking probabilities show very limited variations for both SREBO and AIREBO (cf. Fig. 9).

2. Sticking probability as function of the incident and azimuthal angles θ_v and φ_v

The effects of the incidence and the azimuthal angles were investigated for SREBO and AIREBO. Similar radial distributions of the sticking probability were obtained for the two potentials. Also, the azimuthal variation of the sticking probability was investigated for a collision energy of 0.1 eV, and three values of θ_v: 165°, 170° and 190°. For each of these values, trajectory simulations were performed for 12 values of φ_v ($k \times \frac{\pi}{6}$, k = 0, 1, 2, . . .). The results showed that the sticking probability does not depend on φ_v.

Therefore, we only discuss the variations of the sticking probabilities with the incidence angle calculated with SREBO for C_{36} and C_{80}.

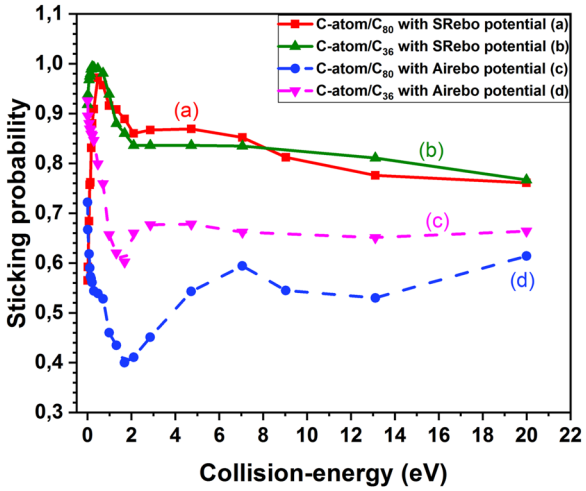

FIG. 9. Variations of the overall sticking probabilities for C–C_{36} and C–C_{80} as a function of the collision-energy of the projectile atoms, obtained with SREBO [straight line (a) and (b)] and AIREBO [dashed line (c) and (d)].

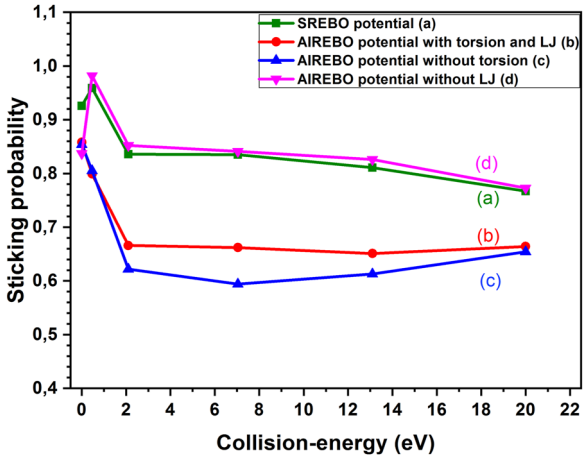

FIG. 11. Variations of the overall sticking probabilities for C–C_{36} as a function of the collision-energy of the projectile atoms calculated with SREBO, AIREBO with both LJ interaction and torsional effect, AIREBO without LJ and AIREBO without torsional effect.

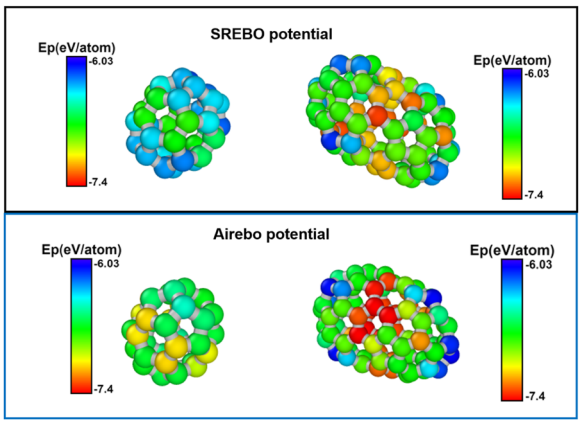

FIG. 10. Snapshot of the potential energy, also called atomic potential energy, for each atom in the structure after 10 ns of equilibration at 300 K.Carbon atoms are colored according to their potential energy.

Figure 12 shows the variations of the sticking probabilities, i.e., $\langle p_{sticking}\rangle_{\theta_v,\varphi_v}(\varepsilon_{col},\theta_v,\varphi_v)$, of C-atom on C_{36} [(a)] and C_{80} [(b)] fullerenes as function of the impact angle θ_v, for two values of the azimuthal angle, $\varphi_v = 0$ and $\varphi_v = \pi$, and four values of the collision-energy, i.e., 0.1; 0.13; 0.17 and 0.21 eV. Results show that in the case of C_{36} and for all the investigated values of φ_v and collision-energy, the sticking probability is almost constant and equal to 1 when the projectile enters the interaction sphere with an angle below 20° with respect to the normal to the sphere, i.e. θ_v between 160° and 180°. The sticking probability decreases very sharply for θ_v below 160° and reaches zero when the projectile enters the interaction sphere with an angle of 30° with respect to the normal to the interaction sphere, i.e., $\theta_v \approx 150°$. The value of the sticking probabilities significantly depends on the collision energy in the region $\approx 150° < \theta_v < 160°$. Lower kinetic energy projectiles are more likely captured by the cluster.

Overall, the results obtained for C_{80} are similar [Fig. 12(b)] with an azimuthal symmetry of the sticking probability, a large sticking probability for impact angles below 20°, i.e., θ_v between 160° and 180°, a sharp decrease of the sticking probability over a 10° range of the impact angle, i.e., θ_v between 150° and 160°, and zero sticking probability for impact angles larger than 30°, i.e., θ_v less than 150°.

E. C–C_{36} and C–C_{80} sticking cross-section

The sticking cross-sections were estimated from the average sticking probabilities using Eq. (5). The sticking cross-sections obtained for the four energy values typical of carbon nanostructures synthesis environment are given in Table I. In the case of C_{36}, the two investigated potentials yield similar values for the sticking cross-section, in the range 120–140 $Å^2$, except for the largest energy value considered in this work. However, the cross-section calculated with SREBO decreases with the collision energy, while the one obtained with AIREBO shows almost no dependence on the collision energy. In the case of the C_{80}, the two investigated potentials yield significantly different cross-section values. SREBO tends to predict cross-section values 30% larger than those obtained with AIREBO. Also, the two potentials give different variation trends. While SREBO yields monotonous increase of the cross-section as function of the energy, the cross-section obtained with AIREBO do not show any clear variation trend.

Besides, the simulations performed with SREBO result in similar cross-section values for C_{36} and C_{80} at low energy (0.10 and 0.13 eV) and significantly larger cross-section value for C_{80} at high energy (0.17 and 0.21 eV). The results are different for AIREBO that predicts significantly larger cross-section values for C_{36} over all the investigated energy range. This difference is a direct consequence of the probability variation trend for the surface-sticking configurations discussed in Sec. IV D 1 (cf. Fig. 9).

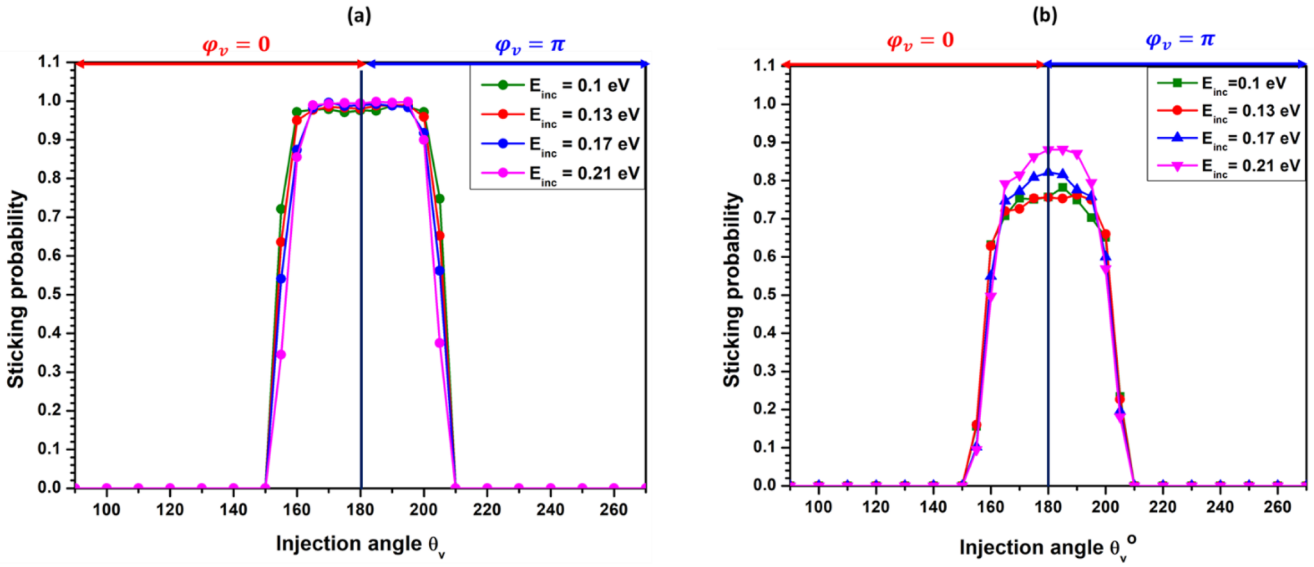

FIG. 12. Variation of the sticking probability as a function of the injection angle θ_v calculated with SREBO for C_{36} (a) and C_{80} (b).

TABLE I. C–C_{36} and C–C_{80} sticking cross-sections calculated with SREBO and AIREBO for different collision energies.

	Sticking cross-section of C–C_{36} (cm^2)		Sticking cross-section of C–C_{80} (cm^2)	
Collision-energy (eV)	SREBO	AIREBO	SREBO	AIREBO
0.10	1.40×10^{-14}	1.34×10^{-14}	1.30×10^{-14}	1.03×10^{-14}
0.13	1.37×10^{-14}	1.34×10^{-14}	1.35×10^{-14}	0.94×10^{-14}
0.17	1.31×10^{-14}	1.33×10^{-14}	1.54×10^{-14}	0.98×10^{-14}
0.21	1.17×10^{-14}	1.34×10^{-14}	1.70×10^{-14}	0.92×10^{-14}

V. CONCLUSION

Classical molecular dynamics simulations were performed in order to study the mechanisms of carbon atom sticking to C_{36} and C_{80} carbon fullerenes. We focused on the analysis of the interaction dynamics, the identification of the different sticking configurations, the determination of the corresponding sticking probabilities and the overall sticking cross-sections. We compared the results obtained with SREBO and AIREBO interaction potentials, to emphasize long range interactions and torsional effects.

We showed the existence of a variety of sticking mechanisms. When SREBO potential is used, the sticking process mainly results in a surface-sticking and 2N-sticking configurations for collision-energy in the thermal range, i.e., from 5×10^{-3} to 0.2 eV. The reaction route leading to the 2N-sticking configuration where the projectile is fully integrated in the fullerene structure is activated even at very low energy. The surface-sticking configuration becomes unlikely at high collision-energy, typically above 15 eV. We showed that a fullerene structure can be recovered by an annealing at 2000 K. Except in the case of the surface-sticking configuration, the sticking mechanism always involves the formation of highly unstable structures containing one or more large cycle defects and, less frequently, three atom-cycles. Most of these defects can be readily eliminated by annealing.

Taking into account the LJ interaction with AIREBO leads to a significant change in the interaction dynamics. Typically, these interactions tend to favor the surface-sticking configuration over a wide range of collision energy, i.e. up to 10 eV. The probability to obtain this configuration remains significant even at collision energy as high as 20 eV. There are several reaction routes that lead to this configuration, the dominant one depending on the collision energy. At low energy, i.e. below 2 eV, this configuration is obtained by a single step addition process as in the case of SREBO. At larger energy, it is obtained by multi-step processes that were not observed with SREBO. The activation of the reaction routes leading to 2N-sticking configuration requires large energy (~2 eV) with AIREBO. The probabilities of 2N- and 3N-sticking configurations are lower than in the case of SREBO.

The differences in the interaction mechanism and the partial sticking probability for the different configurations observed with

SREBO and AIREBO results in very different trends in the variation of the overall sticking probability with the collision-energy. However, the simulations performed with both potentials predict almost constant sticking probability-values for collision-energy values larger than 2–4 eV. The most significant sticking probability variation are observed between 5×10^{-3} – 2 eV for both potentials, even though the corresponding variation trends are different.

The sticking cross-sections determined for C_{36} and C_{80} with SREBO are fairly close, and are respectively, factors 3 and 5, greater than the geometrical cross-section. Their variations as function of the collision-energy show however opposite behaviors, since the sticking cross-section decreases with energy for C_{36} while it increases for C_{80}. These results tend to show that sticking upon a collision to a larger cluster is less likely. However, a larger cluster size tends to compensate for the lower sticking probability. The sticking cross-section for C_{36} obtained with AIREBO show similar value. This is not the case for C_{80} for which the sticking cross-section obtained with AIREBO are significantly lower than the value obtained by SREBO. These results show that taking into account the long-range interactions tends to stabilize the cluster and to decrease the sticking probability, and this effect is much more pronounced for larger cluster.

Our results, and in particular the cross-section values obtained, show that the growth of both fullerenes may proceed through reactions with C-atom. As a matter of fact, the projectile atom can be always easily integrated to the fullerene target structures after a simulated annealing at a temperature of 2000 K. Such annealing may be ensured by collisions with thermal or moderate energy species in non-equilibrium discharge plasmas used for the synthesis of carbon structures. It appears therefore that the contribution of C-atom to cluster growth in these discharges is mainly related to its density level as compared to other possible precursor species, e.g. C_2.

SUPPLEMENTARY MATERIAL

The number of simulations necessary to achieve statistically significant values for the sticking probability was determined by performing a large set of simulations for different values of the collision-energy. The details of this study are given in the supplementary material.

ACKNOWLEDGMENTS

This work was partially supported by the ANR MONA project, Grant No. ANR-18-CE30-0016-02 of the French "Agence Nationale de la Recherche, the French Fédération de Recherche sur la Fusion Magnétique Contrôlée FRFMC. One of the authors (K.H.) acknowledges the support of Institut Universitaire de France."

AUTHOR DECLARATIONS

Conflict of Interest

The authors have no conflicts to disclose.

Author Contributions

A. Allouch: Conceptualization (equal); Formal analysis (equal); Investigation (equal); Methodology (equal); Software (equal); Validation (equal); Visualization (equal); Writing – original draft (equal); Writing – review & editing (equal). **J. Mougenot**: Conceptualization (equal); Investigation (equal); Methodology (equal); Software (equal); Supervision (equal); Writing – review & editing (equal). **A. Michau**: Conceptualization (supporting); Resources (supporting); Validation (supporting); Writing – review & editing (supporting). **S. Prasanna**: Resources (supporting); Validation (supporting); Writing – review & editing (supporting). **P. Brault**: Methodology (supporting); Validation (supporting); Writing – review & editing (supporting). **F. Maurel**: Methodology (supporting); Validation (supporting); Writing – review & editing (supporting). **K. Hassouni**: Conceptualization (equal); Formal analysis (equal); Funding acquisition (equal); Investigation (equal); Methodology (equal); Resources (equal); Supervision (equal); Validation (equal); Writing – review & editing (equal).

DATA AVAILABILITY

The data that support the findings of this study are available from the corresponding author upon reasonable request.

REFERENCES

Afanas'ev, D., Dyuzhev, G., and Kruglikov, A., "Carbon flows from an arc discharge in regimes optimum for production of fullerenes," Tech. Phys. **46**(5), 638–639 (2001).

Alekseev, N. and Dyuzhev, G., "Production of fullerenes in gas discharge plasmas. I. Kinetics of fullerene formation from polycyclic structures," Tech. Phys. **44**(9), 1093–1097 (1999).

Alekseev, N., Chibante. F., and Dyuzhev, G., "On the transformation of carbon vapor in the gas-plasma jet of an arc discharge," Tech. Phys. **46**(6), 761–766 (2001).

Allouch, A., Mougenot, J., Prasanna, S., Michau, A., Seydou, M., Maurel, F., Brault, P., and Hassouni, K., "Statistical abundance and stability of carbon nanostructures by combined condensation-annealing molecular dynamics simulations," Comput. Theor. Chem. **1201**, 113252 (2021).

Arnas, C., Martin, C., Roubin P., Pégourié, B., De Temmerman, G., Hassouni, K., Michau, A., Lombardi, G., and Bonnin, X., "Similarities and differences between dust produced in laboratory plasmas and in the mast and tore supra tokamaks," Plasma Phys. Control. Fusion **52**(12), 124007 (2010).

Bernholc, J. and Phillips, J., "Kinetics of aggregation of carbon clusters," Phys. Rev. B **33**(10), 7395 (1986).

Borand, G., Akçamlı, N., and Uzunsoy, D., "Structural characterization of graphene nanostructures produced via arc discharge method," Ceram. Int. **47**(6), 8044–8052 (2021).

Bratovcic, A., "Biomedical application of nanocomposites based on fullerenes-C60," in *New Technologies, Development and Application VI* (Springer, 2023), Vol. 2, pp. 107–117.

Brenner, D. W., "Empirical potential for hydrocarbons for use in simulating the chemical vapor deposition of diamond films," Phys. Rev. B **42**(15), 9458 (1990).

Brenner, D., Shenderova, O., Harrison, J., Stuart, S., Ni, B., and Sinnott, S., "A second-generation reactive empirical bond order (REBO) potential energy expression for hydrocarbons," J. Phys.: Condens. Matter **14**(4), 783–802 (2002).

Cai, W., Xu, L., Shao, N., Shao, X., and Guo, Q., "An efficient approach for theoretical study on the low-energy isomers of large fullerenes C90–C140," J. Chem. Phys. **122**(18), 184318 (2005).

Celaya, C. A., Muñiz, J., and Sansores, L. E., "New nanostructures of carbon: Quasi-fullerenes C_{n-q} (n = 20, 42, 48, 60)," Comput. Theor. Chem. **1117**, 20–29 (2017).

Dominique, C. and Arnas, C., "Cathode sputtering and the resulting formation of carbon nanometer-size dust," J. Appl. Phys. **101**(12), 123304 (2007).

Dzhurakhalov, A. A., Stelmakh, V. G., and Yadgarov, I. D., "Computer simulation of the interaction of ringlike carbon clusters with nanographene," J. Phys.: Conf. Ser. **640**(1), 012023 (2015).

Farhat, S. and Scott, C. D., "Review of the arc process modeling for fullerene and nanotube production," J. Nanosci. Nanotechnol. **6**(5), 1189–1210 (2006).

Furche, F. and Ahlrichs, R., "Fullerene C80: Are there still more isomers?," J. Chem. Phys. **114**(23), 10362–10367 (2001).

Gao, J., Lin, Z.-Z., and Ning, X.-J., "Isomers of C36 and free energy criteria for cluster growth," J. Chem. Phys. **126**(17), 174309 (2007).

Hosseini-Hashemi, S., Sepahi-Boroujeni, A., and Sepahi-Boroujeni, S., "Analytical and molecular dynamics studies on the impact loading of single-layered graphene sheet by fullerene," Appl. Surf. Sci. **437**, 366–374 (2018).

Jones, R. O., "Density functional study of carbon clusters C_{2n} ($2 \le n \le 16$). I. Structure and bonding in the neutral clusters," J. Chem. Phys. **110**(11), 5189–5200 (1999).

Kosimov, D., Dzhurakhalov, A., and Peeters, F., "Carbon clusters: From ring structures to nanographene," Phys. Rev. B **81**(19), 195414 (2010).

Lai, S., Setiyawati, I., Yen, T., and Tang, Y., "Studying lowest energy structures of carbon clusters by bond-order empirical potentials," Theor. Chem. Acc. **136**, 20 (2017).

Michau, A., Arnas, C., Lombardi, G., Bonnin, X., and Hassouni, K., "Nanoparticle formation and dusty plasma effects in DC sputtering discharge with graphite cathode," Plasma Sources Sci. Technol. **25**(1), 015019 (2016a).

Michau, A., Hassouni, K., Arnas, C., and Lombardi, G., "On the competition between the phenomena involved in the aerosol dynamics in sputtering nonequilibrium plasma," IEEE Trans. Plasma Sci. **44**(4), 528–534 (2016b).

Ning, N., Couedel, L., Arnas, C., and Khrapak, S., "Computational prediction of rate constants for reactions involved in Al clustering," J. Phys. Chem. A **121**(44), 8333–8340 (2017).

Novikov, P. V., Osipova, I. V., Churilov, G. N., and Dudnik, A. I., "Simulation of fullerene formation in a carbon-helium plasma," Fullerenes, Nanotubes Carbon Nanostruct. **29**(5), 337–342 (2021).

Paukov, M., Kramberger. C., Begichev, I., Kharlamova, M., and Burdanova, M., "Functionalized fullerenes and their applications in electrochemistry, solar cells, and nanoelectronics," Materials **16**(3), 1276 (2023).

Perez-Mellor, A. F., Parneix, P., Calvo, F., and Falvo, C., "Finite-temperature stability of hydrocarbons: Fullerenes vs flakes," J. Chem. Phys. **157**(17), 171102 (2022).

Rao, N., Singh, R., and Bashambu, L., "Carbon-based nanomaterials: Synthesis and prospective applications," Mater. Today: Proc. **44**, 608–614 (2021).

Rysaeva, L. K., Lobzenko, I. P., Baimova, J. A., Dmitriev, S. V., and Zhou, K., "Modeling C540-C20 fullerene collisions," Rev. Adv. Mater. Sci. **57**(2), 143–150 (2018).

Schwiegert, V. A., Alexandrov, A. L., Morokov, Y. N., and Bedanov, V. M., "Kinetics of carbon cluster isomerization: From tricylic rings to fullerenes," Chem. Phys. Lett. **235**(3-4), 221–229 (1995).

Sharma, S., Kumar, P., and Chandra, R., "Introduction to molecular dynamics," in *Molecular Dynamics Simulation of Nanocomposites using BIOVIA Materials Studio, Lammps and Gromacs* (Elsevier, 2019), pp. 1–38.

Stuart, S. J., Tutein, A. B., and Harrison, J. A., "A reactive potential for hydrocarbons with intermolecular interactions," J. Chem. Phys. **112**(14), 6472–6486 (2000).

Ueno, Y. and Saito, S., "Geometries, stabilities, and reactions of carbon clusters: Towards a microscopic theory of fullerene formation," Phys. Rev. B **77**(8), 085403 (2008).

Ulukmuradov, A., Yadgarov, I., Stelmakh, V., and Umarov, F., "Computer simulation of adsorption of fullerene on graphene," J. Nano. Electron. Phys. **13**(2), 02025 (2021).

Wang, C., Li, D., Lu, Z., Song, M., and Xia, W., "Synthesis of carbon nanoparticles in a non-thermal plasma process," Chem. Eng. Sci. **227**, 115921 (2020).

Yamaguchi, Y. and Maruyama, S., "A molecular dynamics simulation of the fullerene formation process," Chem. Phys. Lett. **286**(3-4), 336–342 (1998).

Yang, K., Zhang, F., Chen, Y., Zhang, H., Xiong, B., and Chen, H., "Recent progress on carbon-based composites in multidimensional applications," in *Composites Part A: Applied Science and Manufacturing* (Elsevier, 2022), Vol. 157, p. 106906.

Zhang, W., Xu, Z., and Zhu, Z., "Study of thermal stability of fullerenes by molecular dynamics," Int. J. Mod. Phys. B **19**(15n17), 2892–2898 (2005).